nature medicine

A rare mutation in *UNC5C* predisposes to late-onset Alzheimer's disease and increases neuronal cell death

Monica K Wetzel-Smith[1,21], Julie Hunkapiller[2,21], Tushar R Bhangale[3], Karpagam Srinivasan[1], Janice A Maloney[1], Jasvinder K Atwal[1], Susan M Sa[4], Murat B Yaylaoglu[4], Oded Foreman[4], Ward Ortmann[2], Nisha Rathore[2], David V Hansen[1], Marc Tessier-Lavigne[5], Alzheimer's Disease Genetics Consortium[6], Richard Mayeux[7,8], Margaret Pericak-Vance[9,10], Jonathan Haines[11], Lindsay A Farrer[12–16], Gerard D Schellenberg[17], Alison Goate[18–20], Timothy W Behrens[2], Carlos Cruchaga[18,20], Ryan J Watts[1] & Robert R Graham[2]

We have identified a rare coding mutation, T835M (rs137875858), in the *UNC5C* netrin receptor gene that segregated with disease in an autosomal dominant pattern in two families enriched for late-onset Alzheimer's disease and that was associated with disease across four large case-control cohorts (odds ratio = 2.15, P_{meta} = 0.0095). T835M alters a conserved residue in the hinge region of UNC5C, and *in vitro* studies demonstrate that this mutation leads to increased cell death in human HEK293T cells and in rodent neurons. Furthermore, neurons expressing T835M UNC5C are more susceptible to cell death from multiple neurotoxic stimuli, including β-amyloid (Aβ), glutamate and staurosporine. On the basis of these data and the enriched hippocampal expression of *UNC5C* in the adult nervous system, we propose that one possible mechanism in which T835M *UNC5C* contributes to the risk of Alzheimer's disease is by increasing susceptibility to neuronal cell death, particularly in vulnerable regions of the Alzheimer's disease brain.

Although progress has been made in defining the genetic basis of Alzheimer's disease (AD), much of the heritability of AD remains to be discovered[1–12]. We elected to study a large pedigree in which late-onset AD (LOAD) appeared to segregate in an autosomal dominant pattern and lacked known early-onset AD pathogenic variants[3,13] (**Fig. 1a**). Within this family, there were eight LOAD cases including six autopsy confirmed cases (age of onset ranged from 58 to 85 years (**Supplementary Table 1**)), 15 unaffected family members and four individuals of unknown LOAD status. We performed parametric linkage analysis using a rare dominant model of inheritance and identified several regions that segregated with disease in the pedigree, including a broad peak on chromosome 4 (**Fig. 1b**).

We whole-genome sequenced the DNA from one affected individual (generation III, individual 1) to develop a catalog of variation (**Fig. 1a**). We then applied filters and exclusion criteria to identify candidate variants within the pedigree. We detected a total of 3,827,979 variants in the whole-genome-sequenced sample. We limited the search interval to the five regions with evidence of linkage within the pedigree (**Fig. 1b**, regions with LOD score >1.0 provided in **Supplementary Table 2**). We next applied a series of exclusion criteria to the remaining 98,817 variants (**Supplementary Results**), resulting in a total of 141 variants (**Supplementary Fig. 1**).

The most distantly related affected individual (generation II, individual 7) to the originally sequenced case was exome sequenced to further narrow the number of candidate variants (**Fig. 1a**). Four variants were present in both affected individuals (**Supplementary Table 3**). These four candidate variants included two missense, one synonymous and a 3′ untranslated region variant.

Among the two candidate missense variants is rs1063242, which resides in the coding region for A-kinase anchoring protein 9 (AKAP9, P2979S). Genotyping of rs1063242 in 4,533 LOAD cases and 20,325 controls showed no evidence for enrichment ($P = 0.54$, **Supplementary Table 4**). The remaining candidate missense variant, rs137875858,

[1]Department of Neuroscience, Genentech, South San Francisco, California, USA. [2]Department of Human Genetics, Genentech, South San Francisco, California, USA. [3]Department of Bioinformatics and Computational Biology, Genentech, South San Francisco, California, USA. [4]Department of Pathology, Genentech, South San Francisco, California, USA. [5]Laboratory of Brain Development and Repair, Rockefeller University, New York, New York, USA. [6]http://www.adgenetics.org/. [7]Department of Neurology, Taub Institute on Alzheimer's Disease and the Aging Brain, Columbia University, New York, New York, USA. [8]Gertrude H. Sergievsky Center, Columbia University, New York, New York, USA. [9]The John P. Hussman Institute for Human Genomics, University of Miami, Miami, Florida, USA. [10]Dr. John T. Macdonald Foundation Department of Human Genetics, University of Miami, Miami, Florida, USA. [11]Department of Epidemiology and Biostatistics, Case Western Reserve University, Cleveland, Ohio, USA. [12]Department of Medicine (Biomedical Genetics), Boston University Schools of Medicine and Public Health, Boston, Massachusetts, USA. [13]Department of Neurology, Boston University Schools of Medicine and Public Health, Boston, Massachusetts, USA. [14]Department of Ophthalmology, Boston University Schools of Medicine and Public Health, Boston, Massachusetts, USA. [15]Department of Epidemiology, Boston University Schools of Medicine and Public Health, Boston, Massachusetts, USA. [16]Department of Biostatistics, Boston University Schools of Medicine and Public Health, Boston, Massachusetts, USA. [17]Department of Pathology and Laboratory Medicine, University of Pennsylvania School of Medicine, Philadelphia, Pennsylvania, USA. [18]Department of Psychiatry, Washington University School of Medicine, St. Louis, Missouri, USA. [19]Department of Neurology, Washington University School of Medicine, St. Louis, Missouri, USA. [20]Hope Center for Neurological Disorders, Washington University School of Medicine, St. Louis, Missouri, USA. [21]These authors contributed equally to this work. Correspondence should be addressed to. R.J.W. (rwatts@gene.com), R.R.G. (graham.robert@gene.com) or C.C. (cruchagc@psychiatry.wustl.edu).

Received 23 July; accepted 23 September; published online 24 November 2014; doi:10.1038/nm.3736

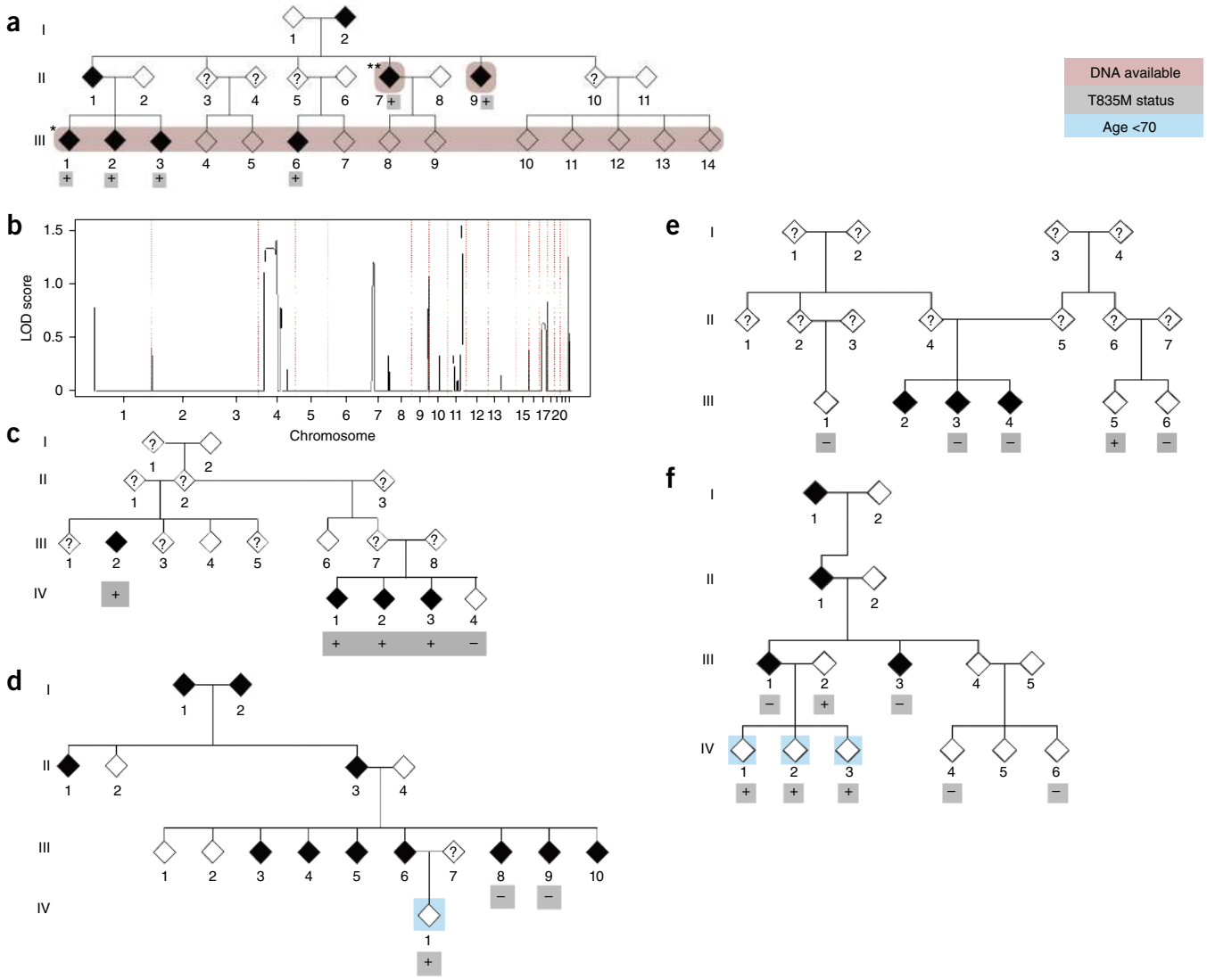

Figure 1 Identification of T835M *UNC5C* as a candidate variant for LOAD. (**a**) A large family with a propensity for developing LOAD was selected for study. Linkage arrays were run on the indicated 16 individuals with available DNA (pink shading). An affected individual (indicated by*) was whole genome sequenced and a second case was exome sequenced (indicated by **). (**b**) Linkage results from the pedigree in **a** using a parametric (rare dominant) model. Five regions segregated with LOAD with a LOD score >1.0. (**c**) A second pedigree in which T835M segregates with LOAD. Heterozygous carriers of T835M are indicated by + and noncarriers by –. (**d**–**f**) Additional LOAD-enriched pedigrees with at least one member heterozygous for T835M *UNC5C* (rs137875858) (**d**,**e** and **f** each represent a different pedigree). Hollow and filled diamonds indicate healthy family members and those diagnosed with AD, respectively. A Taqman assay was used to confirm genotype at T835M (rs137875858).

alters an evolutionarily conserved amino acid in the coding region of *UNC5C* (T835M, **Supplementary Fig. 2a**) and was located in the broad chromosome 4 linkage peak. We confirmed the genotype of rs137875858 within the pedigree by a Taqman assay and the variant was present in all LOAD cases and in two unaffected carriers (ages 75–81 years). UNC5C is a netrin receptor homologous to a protein in *Caenorhabditis elegans* implicated in netrin signaling and contributes to axon guidance during development[14–16]. UNC5C is expressed in neurons in both the developing and adult brain[15,16], and the protein contains a 'death domain' that has been proposed to influence apoptotic signaling. We therefore advanced the T835M *UNC5C* variant for validation in additional LOAD pedigrees and case-control populations.

We screened a cohort of 863 unrelated individuals from pedigrees enriched with familial LOAD for the presence of T835M to identify additional pedigrees for segregation analysis[3,17]. We identified a total of four pedigrees with at least one T835M-heterozygous carrier (**Fig. 1c–f**), and we genotyped their family members for T835M. In one pedigree, the T835M variant completely segregated with disease (**Fig. 1c**), and the family showed evidence of linkage to chromosome 4. Two pedigrees were uninformative for linkage analysis because there was only a single carrier in the pedigree and no informative offspring. In the remaining pedigree, the variant was inherited by three offspring from an unaffected parent but was excluded from the linkage analysis because the three offspring were younger than 70 years old. A possible explanation for the variable penetrance in the pedigrees is the influence of genetic background, which has been observed in both animal models and well-described human risk variants, including *APOE4* (refs. 18,19).

We performed a case-control analysis to test whether T835M *UNC5C* was enriched in individuals with LOAD. The *UNC5C* variant

Study	Case (N chromosomes) T835M	Case (N chromosomes) WT	Control (N chromosomes) T835M	Control (N chromosomes) WT	Odds ratio	95% CI
Genentech study	2	154	1	133	1.73	0.15–19.26
Washington University	1	1,421	5	7,361	1.03	0.12–8.84
ADGC (UPenn)	9	8,121	16	31,816	2.20	0.97–4.99
DeCode Genetics	5	6,387	46	158,450	2.70	1.07–6.79
Fixed-effects model					2.15	1.21–3.84
Random-effects model					2.23	1.26–3.94

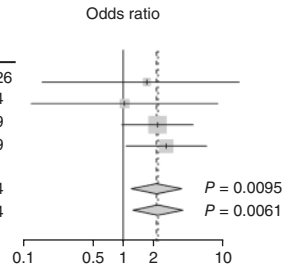

Figure 2 Association of T835M UNC5C (rs137875858) in AD case and control cohorts. The association of T835M UNC5C (rs137875858) is shown in four independent case and control cohorts totaling 8,050 LOAD cases and 98,194 control individuals. The ADGC cohort includes 12,789 additional controls as described in the **Supplementary Results**. CI, confidence interval; N chromosomes, number of chromosomes.

was genotyped in a total of 8,050 cases with LOAD and 98,194 control individuals from four independent data sets (as described in the Online Methods). Using a fixed effects model, T835M *UNC5C* conferred an odds ratio of 2.15 (95% confidence interval of 1.21–3.84) with a *P* value of 0.0095 (**Fig. 2**), supporting the hypothesis that this allele is present at a low frequency in the European population and confers risk for disease.

To dissect the cellular phenotype of the T835M UNC5C mutation we investigated protein expression, cellular localization and cell surface levels by transfecting HEK293T cells. We found little difference between T835M and WT UNC5C, indicating that the T835M mutation is probably not altering protein expression or localization (**Supplementary Fig. 3a–c**). To next test whether the T835M UNC5C mutation may directly alter AD-associated biology[20–22], we examined the effect of UNC5C overexpression on the generation of β-amyloid (Aβ) and extracellular tau. We found that Aβ levels in WT UNC5C– and T835M UNC5C–overexpressing cells were similar to cells expressing a β-galactosidase (β-gal) control vector, indicating that neither WT nor T835M affects amyloid precursor protein (APP) cleavage (**Supplementary Fig. 3d–f**). Additionally, overexpression of T835M or WT UNC5C led to roughly equivalent increases in extracellular tau levels (**Supplementary Fig. 3g,h**), which coincided with the presence of additional cytosolic proteins in the conditioned medium (**Supplementary Fig. 3i**), suggesting that UNC5C expression is probably toxic and induces cell death.

UNC5 family members may drive cell death through their conserved C-terminal death domain[23,24] (**Supplementary Fig. 2b**). Based on the analogous residue in the crystal structure of UNC5B (ref. 25), a related family member, T835M alters the 'hinge' of the closed conformation of UNC5C, suggesting an effect on the death domain of UNC5C. As we observed that UNC5C overexpression led to increased cell death in the extracellular tau experiments, we further explored the cell death phenotype using live-cell imaging. HEK293T cells overexpressing WT UNC5C, T835M UNC5C or a β-gal control vector were longitudinally monitored. Using the IRES-GFP encoded within the constructs, cell confluencies were determined specifically within the transfected cell populations, and growth curves for the transfected cells were generated for each group (**Fig. 3a,b** and **Supplementary Fig. 4**).

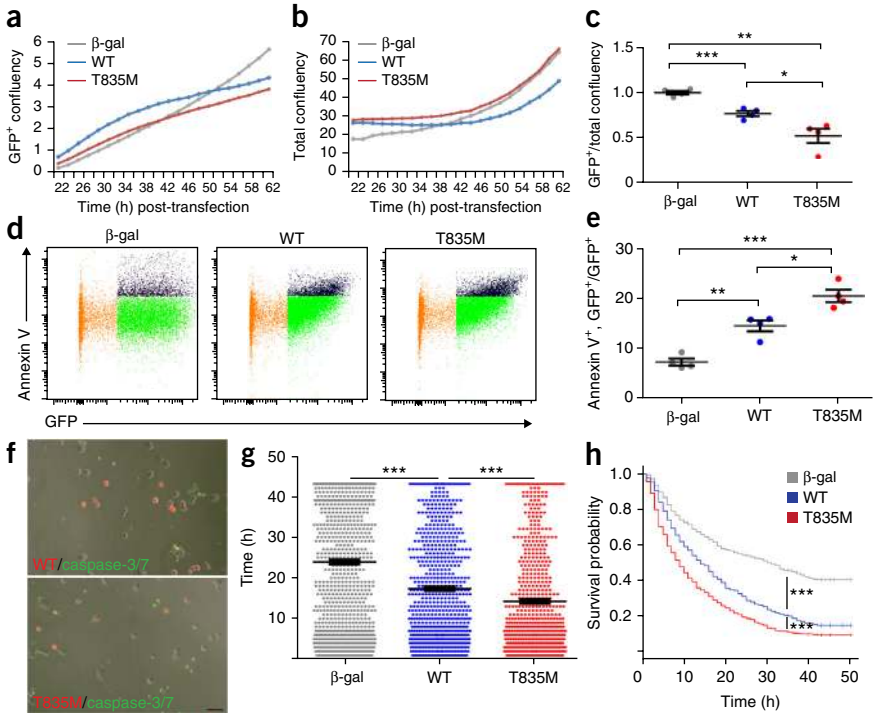

Figure 3 T835M UNC5C increases cell death beyond that induced by WT UNC5C. HEK293T cells were transfected with WT UNC5C, T835M UNC5C or a β-gal control vector, all of which contained an IRES-GFP. (**a**,**b**) Representative growth curves of GFP+ cells (transfected only) (**a**) and total cells (transfected and non-transfected) (**b**). (**c**) Growth of β-gal–, T835M UNC5C– or WT UNC5C–expressing cells. GFP+ specific growth was normalized to total growth, and slopes of the best-fit lines were calculated. Data (**a**–**c**) represent four independent transient transfection experiments with $n = 6$ randomly plated technical replicates per condition for each experiment. $^{***}P = 0.007$, $^{**}P = 0.0011$, $^{*}P = 0.0259$ as analyzed by two-tailed unpaired *t*-test. (**d**) Representative flow cytometry plots of β-gal–, T835M UNC5C– or WT UNC5C–transfected cells analyzed for GFP and annexin V–APC. Orange, untransfected cell population; green, GFP+annexin V− cell population; black, GFP+annexin V+ population. (**e**) Percentage of annexin V+ cells within the GFP+ population representing four independent transient transfection experiments with 100,000 cells analyzed per condition. $^{***}P < 0.0001$, $^{**}P = 0.0014$, $^{*}P = 0.0111$ as analyzed by two-tailed unpaired *t*-test. (**f**) Representative overlay of fluorescent and bright-field images from time-lapse imaging experiments. Red, transfected cells; green, caspase-3/7 activity. Scale bar, 50 μm. (**g**) Average lifetime of cells expressing β-gal ($n = 919$), WT UNC5C ($n = 687$) or T835M UNC5C ($n = 590$) at movie start or that initiated expression during first 20 h of imaging. (**h**) Kaplan-Meier survival curves of cells expressing β-gal ($n = 1,696$), WT UNC5C ($n = 1,085$) or T835M UNC5C ($n = 751$) analyzed by Wald test for *P* values. (**g**,**h**) Data represent three independent transient transfection experiments with $n = 6$ randomly plated technical replicates per experiment and 24 movies per genotype, $^{***}P < 0.0001$, Cox proportional hazards regression model. Data were analyzed with experimenter blinded to samples and represent the mean ± s.e.m.

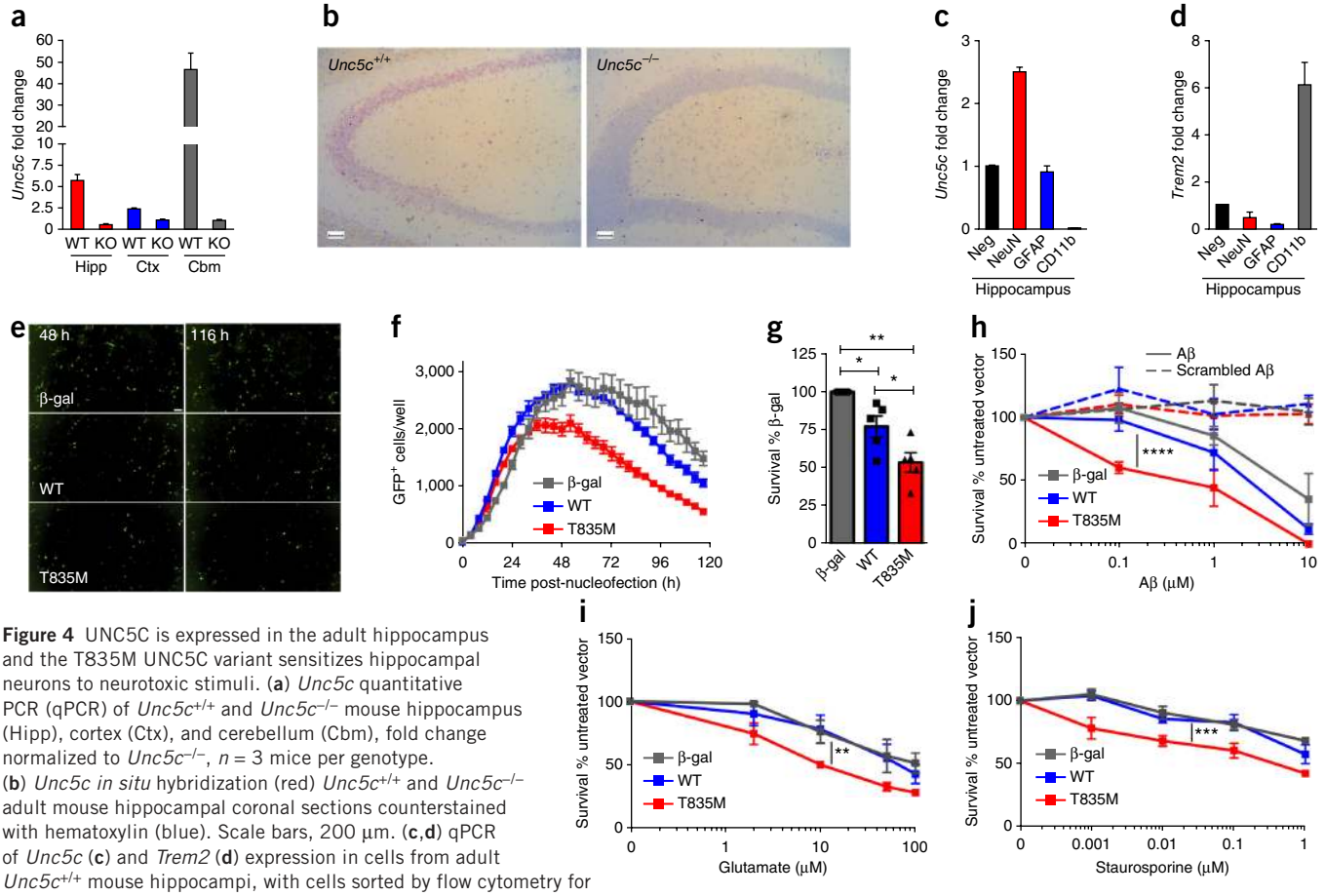

Figure 4 UNC5C is expressed in the adult hippocampus and the T835M UNC5C variant sensitizes hippocampal neurons to neurotoxic stimuli. (**a**) *Unc5c* quantitative PCR (qPCR) of *Unc5c*$^{+/+}$ and *Unc5c*$^{-/-}$ mouse hippocampus (Hipp), cortex (Ctx), and cerebellum (Cbm), fold change normalized to *Unc5c*$^{-/-}$, $n = 3$ mice per genotype. (**b**) *Unc5c in situ* hybridization (red) *Unc5c*$^{+/+}$ and *Unc5c*$^{-/-}$ adult mouse hippocampal coronal sections counterstained with hematoxylin (blue). Scale bars, 200 μm. (**c**,**d**) qPCR of *Unc5c* (**c**) and *Trem2* (**d**) expression in cells from adult *Unc5c*$^{+/+}$ mouse hippocampi, with cells sorted by flow cytometry for neurons (NeuN), astrocytes (GFAP), microglia/macrophages (CD11b) or a non-enriched negative population, fold change normalized to negative population. $n = 3$ *Unc5c*$^{+/+}$ mice total. (**e**) Images of cultured hippocampal neurons expressing β-gal–IRES-GFP, WT UNC5C–IRES-GFP or T835M UNC5C–IRES-GFP at 48 h or 116 h following transfection. Scale bar, 100 μm. (**f**) Number of detected GFP$^+$ cells per well, as a function of time, for the experiment shown in **e**. Each data point is the mean ± s.e.m. of three technical replicates with four fields of view acquired per replicate. (**g**) Survival of WT UNC5C– or T835M UNC5C–transfected neurons, relative to β-gal–transfected neurons, in $n = 5$ independent experiments, as performed in **f**. WT versus T835M UNC5C by two-tailed unpaired *t*-test: $^*P = 0.0394$, or two-tailed one sample *t*-test with β-gal (theoretical mean) versus WT $^*P = 0.0319$ or versus T835M $^{**}P = 0.002$, respectively. (**h**–**j**) β-gal–, WT UNC5C– and T835M UNC5C–IRES-GFP vector expressing hippocampal neurons were challenged with $A\beta_{1-42}$ or scrambled $A\beta_{1-42}$ (**h**) glutamate (**i**) or staurosporine (**j**). Surviving neurotoxin-treated cells were normalized to their respective untreated vector controls. In **h**, $n = 4$ independent neuronal culture experiments, β-gal ($n = 120$ images) versus WT ($n = 120$ images) $P = 0.0609$, WT versus T835M UNC5C ($n = 120$ images) $^{****}P = 1.77\text{x}10^{-9}$, In **i**, $n = 3$ independent experiments, β-gal ($n = 90$ images) versus WT ($n = 90$ images) $P = 0.6032$, WT versus T835M UNC5C ($n = 90$ images) $^{**}P = 0.001446$. In **j**, $n = 3$ independent experiments, β-gal ($n = 90$ images) versus WT ($n = 90$ images) $P = 0.323$, WT versus T835M UNC5C ($n = 90$ images) $^{**}P = 0.0005545$. In **a**,**c**,**d**,**g**–**j**, data are presented as mean ± s.e.m. In **h**–**j**, *P* value is from a likelihood-ratio test comparing two linear mixed models for growth curve analysis (fit using function lmer in the R package lme4): 1. model with the dose-treatment interaction term and 2. model without that term.

We found that growth of WT UNC5C–overexpressing cells was reduced by 25% compared to the β-gal control vector, whereas growth of cells expressing T835M UNC5C was diminished to nearly 50% (**Fig. 3a–c** and **Supplementary Fig. 4**). Furthermore, DNA titration experiments revealed that cells overexpressing WT and T835M UNC5C consistently showed decreased growth compared to those overexpressing β-gal, and cells overexpressing T835M UNC5C grew less than those overexpressing WT UNC5C for all expression levels (**Supplementary Fig. 5a–d**). Differences in cell cycle profiles were not detected between WT UNC5C– and T835M UNC5C–overexpressing cells (**Supplementary Fig. 6**). Taken together, these data indicate that T835M UNC5C either decreased cell growth or increased cell death beyond that of WT UNC5C even at low expression levels.

To investigate the cell death phenotype in greater depth, we analyzed cell surface expression of annexin V, an early apoptotic marker, and caspase activation in HEK293T cells. We found the percentage of annexin V$^+$ cells within the WT UNC5C–overexpressing population was significantly increased over that of β-gal–overexpressing cells, whereas T835M UNC5C displayed the highest percentage of annexin V$^+$ cells (**Fig. 3d,e** and **Supplementary Fig. 7a–e**). Assaying caspase-3 or caspase-7 activation, one of the hallmark steps in apoptosis, in real time revealed that cells overexpressing WT UNC5C were more likely to spontaneously undergo apoptosis marked by caspase activity than the β-gal–overexpressing control cells, yet T835M UNC5C–overexpressing cells showed an even higher propensity for cell death (**Fig. 3f**, **Supplementary Fig. 8a**, **Supplementary Movies 1–3** and **Supplementary Fig. 8b–d**). Correspondingly, T835M UNC5C decreased the average cell lifetime and substantially reduced survival compared to WT UNC5C (**Fig. 3g,h** and **Supplementary Fig. 8b–d**). Collectively, these data show that the T835M UNC5C AD-linked variant

induces cell death more rapidly and to a higher degree than WT UNC5C in a heterologous cell system.

UNC5C is expressed in the rodent adult nervous system[15] (**Fig. 4a**) and appears to be enriched in neurons of the CA3 hippocampal pyramidal layer (**Fig. 4b**,**c** and **Supplementary Fig. 9a**,**b**), suggesting that UNC5C may have a functional role in these neurons. Moreover, *UNC5C* is expressed in normal human temporal lobe cortical neurons and neurons of the hippocampal pyramidal layer in control subjects and subjects with AD (**Supplementary Fig. 10a**,**b**). Notably, the hippocampus is one of the first regions to degenerate in AD and is required for many types of learning and memory[26–28]. Neuroinflammation may also contribute to AD risk, as has been implicated by the recently described *TREM2* variants[1,6]. To determine whether *UNC5C* is expressed by microglia in the brain or by peripheral blood mononuclear cells (PBMCs), we profiled *UNC5C* expression in adult mouse brain and in subpopulations of mouse and human PBMCs (**Fig. 4c**,**d** and **Supplementary Fig. 9**). Unlike *TREM2*, which is expressed by $CD11b^+$ microglia, monocytes and macrophages, we found little evidence that *UNC5C* is expressed by microglia or PBMCs, suggesting that UNC5C is unlikely to be involved in the inflammatory response during AD.

Given the neuronal expression of *UNC5C*, we next asked whether expression of T835M UNC5C would alter neuronal sensitivity to cell death in cultured primary rat hippocampal neurons. We used a live-cell imaging approach monitoring the time course of expression and basal cell death, which revealed that WT UNC5C–overexpressing neurons were more likely to undergo basal cell death than those overexpressing β-gal, yet T835M UNC5C–overexpressing neurons showed an even higher propensity for cell death (**Fig. 4e–g**, **Supplementary Fig. 11a–c** and **Supplementary Movies 4–6**).

To determine whether T835M UNC5C overexpression may predispose hippocampal neurons to toxic insults like those that occur in AD, we exposed UNC5C variant–overexpressing rat hippocampal neurons to increasing concentrations of the pathogenic peptide $A\beta_{1-42}$ or scrambled $A\beta_{1-42}$ for 48 h. Quantification of immunocytochemistry (**Supplementary Fig. 12**) revealed that T835M UNC5C–overexpressing neurons were more vulnerable to Aβ-induced neurotoxicity than neurons overexpressing WT UNC5C (**Fig. 4h**), whereas there was no difference between WT- and T835M-overexpressing neurons treated with scrambled $A\beta_{1-42}$. To establish whether T835M UNC5C expression confers a broader vulnerability, we challenged UNC5C variant–overexpressing hippocampal neurons to increasing concentrations of glutamate, an excitotoxic neurotransmitter, or staurosporine, a toxic kinase inhibitor. T835M UNC5C–overexpressing neurons were indeed more vulnerable to glutamate- or staurosporine-induced neurotoxicity than neurons overexpressing WT UNC5C (**Fig. 4i**,**j** and **Supplementary Figs. 13** and **14**). These data indicate that neurons overexpressing T835M UNC5C are more prone to cell death in response to multiple neurodegenerative stimuli *in vitro* and that T835M represents a general risk factor for neurotoxins; however, enriched hippocampal expression of UNC5C in the nervous system may result in T835M UNC5C's dominantly inherited risk of neurodegeneration as a result of amyloid accumulation, which is a relatively common pathology. It remains to be determined whether T835M UNC5C is also a risk factor for other neurodegenerative diseases in the context of additional neuronal insults.

Previous AD genetic studies have identified several major pathways implicated in disease, including the Aβ cascade, lipid metabolism and neuroinflammation[1–12]. There are, however, few examples of genetically linked pathways related to neuronal cell death, a hallmark feature of AD. In the present study we provide evidence that the T835M *UNC5C* variant increases AD risk. Of interest, a recent study examined the frequency of coding variants in an exon of *UNC5C* in an AD case-control cohort from China. T835M *UNC5C* was not present in their population; however, there was an aggregation of *UNC5C* rare and predicted deleterious missense variants in AD cases relative to controls[29].

Our cellular data support a mechanism in which T835M UNC5C enhances the susceptibility of neurons to Aβ-mediated cell death. We also observed a general increase in risk to neuronal insults, suggesting that T835M UNC5C may be a risk factor for other neurodegenerative diseases. Nevertheless, the enriched expression of UNC5C in the hippocampus may place T835M carriers at particular risk for AD. We propose that modulation of the UNC5C pathway may represent a new approach to the treatment of AD.

METHODS

Methods and any associated references are available in the online version of the paper.

Note: Any Supplementary Information and Source Data files are available in the online version of the paper.

ACKNOWLEDGMENTS

This work was partially supported by grants from the US National Institutes of Health (R01-AG044546, P50-AG05681), and the Alzheimer's Association (NIRG-11-200110). This research was conducted while C.C. was a recipient of a New Investigator Award in Alzheimer's disease from the American Federation for Aging Research. C.C. is a recipient of a BrightFocus Foundation Alzheimer's Disease Research grant (A2013359S). Samples from the National Cell Repository for Alzheimer's Disease (NCRAD), which receives government support under a cooperative agreement grant (U24 AG21886) awarded by the National Institute on Aging (NIA), were used in this study. NIA-LOAD samples were collected under a cooperative agreement grant (U24 AG026395) awarded by the NIA. The ADGC is funded by the NIA (UO1AG032984). We thank K. Steffansøn and DeCode Genetics for genotype counts of *UNC5C* variants in the Icelandic population, the Alzheimer's Disease Centers, who collected samples used in this study, and patients and their families, whose help and participation made this work possible. We thank J. Norton of the Genetics Core, Washington University. We also thank C. Nelson (Genentech) for the HEK293 wild-type human APP695 stable cell line, K. Hoyte, Y. Lu, M. Sagolla, L. Gilmor, J. Borneo, E. Ladi, J. Grogan, J. Larson and J. Kaminker for technical assistance, and S. Ackerman, The Jackson Laboratory/Howard Hughes Medical Institute, for the generous gift of $Unc5c^{-/-}$ mice.

AUTHOR CONTRIBUTIONS

M.K.W.-S. and J. Hunkapiller designed, conducted and analyzed biological experiments and wrote the manuscript, T.R.B. performed linkage, case-control association, survival, growth-curve and sequencing data analysis, K.S. developed a method for isolating and sorting cell-type-specific adult brain for quantitative PCR, J.A.M. generated vectors and contributed to *in vitro* experiments, J.K.A. supervised the project, S.M.S. performed *Unc5c in situ* hybridization (ISH), M.B.Y. performed *UNC5C* ISH, O.F. contributed to ISH experiments and generated images, N.R. performed sample genotyping and handling and contributed to the manuscript, W.O. coordinated DNA sample collection, sequencing and data management, D.V.H. supervised development of the method for isolating and sorting cell-type-specific adult brain for quantitative PCR, M.T.-L. contributed to the manuscript, the ADGC provided AD case and control cohorts, R.M. provided sample material and contributed to the manuscript, M. P.-V., J. Haines, L.A.F., G.D.S. and A.G. provided sample material and contributed to the manuscript, T.W.B., C.C. and R.J.W. supervised the project and contributed to the manuscript, and R.R.G. supervised the project and wrote the manuscript.

COMPETING FINANCIAL INTERESTS

The authors declare competing financial interests: details are available in the online version of the paper.

1. Coppola, G. *et al.* Evidence for a role of the rare p.A152T variant in *MAPT* in increasing the risk for FTD-spectrum and Alzheimer's diseases. *Hum. Mol. Genet.* **21**, 3500–3512 (2012).
2. Corder, E.H. *et al.* Gene dose of apolipoprotein E type 4 allele and the risk of Alzheimer's disease in late onset families. *Science* **261**, 921–923 (1993).
3. Cruchaga, C. *et al.* Rare variants in *APP*, *PSEN1* and *PSEN2* increase risk for AD in late-onset Alzheimer's disease families. *PLoS ONE* **7**, e31039 (2012).
4. Cruchaga, C. *et al.* Rare coding variants in the phospholipase D3 gene confer risk for Alzheimer's disease. *Nature* **505**, 550–554 (2014).
5. Genin, E. *et al. APOE* and Alzheimer disease: a major gene with semi-dominant inheritance. *Mol. Psychiatry* **16**, 903–907 (2011).
6. Guerreiro, R. *et al. TREM2* variants in Alzheimer's disease. *N. Engl. J. Med.* **368**, 117–127 (2013).
7. Harold, D. *et al.* Genome-wide association study identifies variants at *CLU* and *PICALM* associated with Alzheimer's disease. *Nat. Genet.* **41**, 1088–1093 (2009).
8. Hollingworth, P. *et al.* Common variants at *ABCA7*, *MS4A6A/MS4A4E*, *EPHA1*, *CD33* and *CD2AP* are associated with Alzheimer's disease. *Nat. Genet.* **43**, 429–435 (2011).
9. Jonsson, T. *et al.* A mutation in *APP* protects against Alzheimer's disease and age-related cognitive decline. *Nature* **488**, 96–99 (2012).
10. Jonsson, T. *et al.* Variant of *TREM2* associated with the risk of Alzheimer's disease. *N. Engl. J. Med.* **368**, 107–116 (2013).
11. Lambert, J.C. *et al.* Meta-analysis of 74,046 individuals identifies 11 new susceptibility loci for Alzheimer's disease. *Nat. Genet.* **45**, 1452–1458 (2013).
12. Naj, A.C. *et al.* Common variants at *MS4A4/MS4A6E*, *CD2AP*, *CD33* and *EPHA1* are associated with late-onset Alzheimer's disease. *Nat. Genet.* **43**, 436–441 (2011).
13. Harms, M. *et al.* C9orf72 hexanucleotide repeat expansions in clinical Alzheimer disease. *JAMA Neurol.* **70**, 736–741 (2013).
14. Leonardo, E.D. *et al.* Vertebrate homologues of *C. elegans* UNC-5 are candidate netrin receptors. *Nature* **386**, 833–838 (1997).
15. Ackerman, S.L. *et al.* The mouse rostral cerebellar malformation gene encodes an UNC-5-like protein. *Nature* **386**, 838–842 (1997).
16. Przyborski, S.A., Knowles, B. & Ackerman, S. Embryonic phenotype of *Unc5h3* mutant mice suggests chemorepulsion during the formation of the rostral cerebellar boundary. *Development* **125**, 41–50 (1998).
17. Wijsman, E.M. *et al.* Genome-wide association of familial late-onset Alzheimer's disease replicates BIN1 and CLU and nominates CUGBP2 in interaction with APOE. *PLoS Genet.* **7**, e1001308 (2011).
18. Lee, J.H., Cheng, R., Graff-Radford, N., Foroud, T. & Mayeux, R. Analyses of the National Institute on Aging Late-Onset Alzheimer's Disease Family Study: implication of additional loci. *Arch. Neurol.* **65**, 1518–1526 (2008).
19. Nadeau, J.H. Modifier genes and protective alleles in humans and mice. *Curr. Opin. Genet. Dev.* **13**, 290–295 (2003).
20. Goedert, M., Spillantini, M.G., Cairns, N.J. & Crowther, R.A. Tau proteins of Alzheimer paired helical filaments: abnormal phosphorylation of all six brain isoforms. *Neuron* **8**, 159–168 (1992).
21. Glenner, G.G. & Wong, C.W. Alzheimer's disease: initial report of the purification and characterization of a novel cerebrovascular amyloid protein. *Biochem. Biophys. Res. Commun.* **120**, 885–890 (1984).
22. Masters, C.L. *et al.* Neuronal origin of a cerebral amyloid: neurofibrillary tangles of Alzheimer's disease contain the same protein as the amyloid of plaque cores and blood vessels. *EMBO J.* **4**, 2757–2763 (1985).
23. Llambi, F., Causeret, F., Bloch-Gallego, E. & Mehlen, P. Netrin-1 acts as a survival factor via its receptors UNC5H and DCC. *EMBO J.* **20**, 2715–2722 (2001).
24. Thiebault, K. *et al.* The netrin-1 receptors UNC5H are putative tumor suppressors controlling cell death commitment. *Proc. Natl. Acad. Sci. USA* **100**, 4173–4178 (2003).
25. Wang, R. *et al.* Autoinhibition of UNC5b revealed by the cytoplasmic domain structure of the receptor. *Mol. Cell* **33**, 692–703 (2009).
26. Braak, H., Braak, E. & Bohl, J. Staging of Alzheimer-related cortical destruction. *Eur. Neurol.* **33**, 403–408 (1993).
27. Ball, M.J. Neuronal loss, neurofibrillary tangles and granulovacuolar degeneration in the hippocampus with ageing and dementia. A quantitative study. *Acta Neuropathol.* **37**, 111–118 (1977).
28. Squire, L.R. Memory and the hippocampus: a synthesis from findings with rats, monkeys, and humans. *Psychol. Rev.* **99**, 195–231 (1992).
29. Jiao, B. *et al.* Investigation *of TREM2*, *PLD3*, *and UNC5C* variants in patients with Alzheimer's disease from mainland China. *Neurobiol. Aging* **35**, 2422.e9–2422.e11 (2014).

ONLINE METHODS

Human subjects. All human samples used in this study have been included in previous publications[12,17]. All patients were recruited after providing informed consent and with approval by the participating institutional review boards, and the study was conducted according to the principles expressed in the Declaration of Helsinki. Regardless of the source (NIA-LOAD Family Study or NCRAD), patients and families were required to meet the same study criteria[17]. The ADGC assembled a discovery data set (stage 1, 8,309 individuals with LOAD (cases) and 7,366 cognitively normal elders (CNEs) as controls) using data from eight cohorts and a ninth newly assembled cohort from the 29 National Institute on Aging (NIA)-funded Alzheimer Disease Centers (ADCs), with data coordinated by the National Alzheimer Coordinating Center (NACC) and samples coordinated by the National Cell Repository for Alzheimer Disease (NCRAD)[12]. Written informed consent was obtained from study participants or, for those with substantial cognitive impairment, from a caregiver, legal guardian or other proxy, and the study protocols for all populations were reviewed and approved by the appropriate institutional review boards.

Linkage analysis. A pedigree (**Fig. 1a**) from a previously described cohort[3,17] with apparent autosomal dominant inheritance of LOAD was selected for study and screened for known pathogenic variants in *APP*, *PSEN1*, *PSEN2*, *MAPT*, *GRN* and *TREM2*.

DNA was available for 16 members of the family described in **Figure 1a**. Samples were genotyped using Illumina InfiniumLinkage24 SNP array (5,913 SNPs). Using this SNP data, relationships between the individuals were verified by examining kinship coefficients between each sample-pair estimated using PLINK using "–genome option"[30]. For computational feasibility, this large pedigree was split into two subgroups using the software PedCut[31] and the 'maxbit 23' option. SNPs that showed Mendelian errors were identified and removed using Pedwipe software[32]. Parametric linkage analysis was performed on these data using Merlin[32] and a rare disease with partially-dominant inheritance model with penetrance probabilities: 0.0001, 0.8 and 0.8 and disease prevalence of 0.0001.

Sequencing data analysis. Whole-genome sequencing followed by data quality control (QC), short-read alignment and variant calling was performed on an affected individual III, 1 (**Fig. 1a**) by "unchained combinatorial probe anchor ligation sequencing," as described previously[33]. Agilent-based exome capture and short-read sequencing using Illumina Hi-Seq was performed on a second affected individual (II,5) from the pedigree (**Fig. 1a**). Resulting reads were aligned to reference genome using BWA[34]. QC of these data was performed using GATK[35] and involved removal of PCR duplicates, quality recalibration, and realignment around short indels. Variant calling was also performed using GATK. Variants from both samples were annotated for potential function using Annovar[36].

LOAD pedigree collection. An additional 863 samples selected from the LOAD family cohort[17,3] were genotyped for i T835M using an Illumina Golden Gate Assay. Family members of individuals heterozygous for *UNC5C* T835M were then genotyped via Kompetitive Allele Specific PCR (KASPar) technology, as previously described[37–39].

Reverse primer: TGCTGGATCCTGCGAACAC, forward primer: GGGAG AGGGATGCTGAAAGC, reporter primer 1: CCCGTGACCGTGGTGA, reporter primer 2: CCCGTGACCATGGTGA.

LOAD association study sample information. Several independent LOAD case-control collections were genotyped for UNC5C T835M. A cohort of 78 APOE4$^+$ cases and 67 APOE4$^+$ population-matched controls with no evidence of disease with a minimum age of 75 years and genotype was determined at *UNC5C* T835M from whole genome and exome sequencing data. A previously described collection of 711 LOAD cases and 3,683 age-matched controls using KASPar as described above[37–39]. A collection of 4,065 LOAD cases and 3,127 age-matched controls were genotyped and passed QC using the Illumina exome array v1.0.

The NIA ADC samples. The NIA ADC cohort, assembled by the Alzheimer's Disease Genetics Consortium (ADGC), included subjects ascertained and evaluated by the clinical and neuropathology cores of the 29 NIA-funded ADCs. Data collection is coordinated by the National Alzheimer's Coordinating Center (NACC). NACC coordinates collection of phenotype data from the 29 ADCs, cleans all data, coordinates implementation of definitions of AD cases and controls, and coordinates collection of samples. The ADC cohort consists of 2,499 autopsy-confirmed and 1,748 clinically confirmed AD cases, 175 cognitively normal elders (CNEs) with complete neuropathology data who were older than 60 years at age of death, and 2,669 living CNEs evaluated using the Uniform data set (UDS) protocol[40,41] who were documented to not have mild cognitive impairment (MCI) and were between 60 and 100 years of age at assessment. Among cases, the average age at onset was 71.6 years (±9.0 years), and *APOE* genotypes were 0.1% e22, 3.5% e23, 31.6% e33, 2.8% e24, 44.3% e34, and 14.7% e44. Among controls, the average age at last exam was 76.6 years (±9.4 years), and *APOE* genotypes were 0.7% e22, 13.0% e23, 56.8% e33, 2.1% e24, 21.4% e34, and 2.2% e44. Based on the data collected by NACC, the ADGC Neuropathology Core Leaders Subcommittee derived inclusion and exclusion criteria for AD and control samples. All autopsied subjects were age ≥60 years at death. AD cases had dementia according to DSM-IV criteria or Clinical Dementia Rating (CDR) ≥1. Neuropathologic stratification of cases followed NIA/Reagan criteria explicitly or used a similar approach when NIA/Reagan criteria[42] were coded as not done, missing, or unknown. Cases were intermediate or high likelihood by NIA/Reagan criteria with moderate to frequent amyloid plaques and neurofibrillary tangle (NFT) Braak stage of III–VI (refs. 40,41). Persons with Down's syndrome, non-AD tauopathies and synucleinopathies were excluded. All autopsied controls had a clinical evaluation within 2 years of death. Controls did not meet DSM-IV criteria for dementia, did not have a diagnosis of mild cognitive impairment (MCI), and had a CDR of 0, if performed. Controls did not meet or were low-likelihood AD by NIA/Reagan criteria, had sparse or no amyloid plaques, and a Braak NFT stage of 0–II. ADCs sent frozen tissue from autopsied subjects and DNA samples from some autopsied subjects and from living subjects to the ADCs to the National Cell Repository for Alzheimer's Disease (NCRAD). DNA was prepared by NCRAD and sent either by NCRAD or by the University of Pennsylvania and sent to the North Shore Medical Center for genotyping. An additional 12,789 controls were genotyped using the Illumina exome array v1.0. Genetic outliers were removed based on Eigenvectors from Principal Component Analysis using Eigenstrat (sigma >6)[43]. A total of 3,196 LOAD cases and 79,248 control individuals from Iceland (DeCode Genetics) were genotyped and imputed for T835M as described[9].

Meta-analysis. Association and meta-analysis of case-control data (**Fig. 1d**) was performed using the function metabin in the R (http://www.r-project.org/) package meta (http://cran.r-project.org/package=meta) using the default parameters, which apply the Mantel-Haenszel inverse variance weighting method for pooling. Using this function we compared risk allele counts in cases and controls in the four genotyped cohorts and performed fixed as well as random-effect meta analyses.

Genotyping. A custom Taqman SNP genotyping assay for T835M *UNC5C* with two allele-specific TaqMan MGB probes containing distinct fluorescent dyes (Probe1-VIC CCCGTGACCGTGGTGA and Probe2- FAM CCCGTGACCATGGTGA) and a PCR primer pair (Forward Primer GGG AGAGGGATGCTGAAAGC and Reverse Primer TGCTGGATCCTGCG AACAC) was designed and used to genotype all 16 members of the pedigree (**Fig. 1a**).

Plasmid constructs. UNC5C-IRES-GFP or UNC5C-IRES-DsRed vector containing human *UNC5C* full-length coding sequence was used as template for insertion of the T835M mutant allele using the Quick-change site-directed mutagenesis kit (Stratagene, Agilent Technologies). Human T835M mutant allele 5′ primer sequence: GAACACCATCACCA**T**GGTCACGGGGCC. Either β-gal-IRES-GFP or β-gal-IRES-DsRed was used as negative control vector.

doi:10.1038/nm.3736

To assay tau release into extracellular medium, human wild-type tau 441-amino acid-IRES-GFP was used.

Cell lines. Human embryonic kidney 293T cells (HEK293T) were maintained in high-glucose DMEM supplemented with 10% FBS (Sigma), 1% Glutamax (Gibco, Life technologies), and 1% penicillin/streptomycin (Gibco). Transient transfections of HEK293T cells were performed using X-tremeGENE 9 DNA transfection reagent according to manufacturer's instructions (Roche Diagnostics). HEK293 cells stably expressing wild-type human APP695 were maintained as previously described[44] in DMEM supplemented with 10% FBS (Sigma), 1% glutamax (Gibco), and 1% penicillin/streptomycin (Gibco) and 400 μg mL^{-1} G418 (Cellgro, Corning). Transient transfections of HEK293 wild-type human APP695 stable cell line were performed using Lipofectamine reagent according to manufacturer's instructions (Invitrogen, Life Technologies).

Immunocyctochemistry. HEK293T cells or primary rat hippocampal neurons were fixed with 4% PFA and 4% sucrose in PBS. The cells were permeabilized, blocked, incubated with appropriate primary antibodies anti-UNC5C (1:500, MAB1005, R&D systems)[17], anti-GFP (1:2,000, GFP-1020, Aves Labs, Inc), detected with anti-mouse Alexa 568 (1:1,000, A-11004, Invitrogen), and anti-chicken Alexa 488 secondary antibodies (1:1,000, A-11039, Invitrogen), and then mounted with Prolong gold medium with DAPI nuclear dye (Invitrogen). All digital image acquisition was performed using Leica software linked to a Leica wide-field fluorescent microscope (DM5500; Leica) and CCD camera (DFC360).

Western blot. HEK293T or HEK293 cells stably expressing wild-type human APP695 were plated into six-well plates at 75% confluency and transfected as indicated in the "Cell lines" section. At 24 h post-transfection, cells were split into triplicate. 48 h later, the cells were lysed using RIPA buffer with Complete Protease Inhibitor Cocktail (Roche) and Phospho-stop (Roche). Cell lysates were run on 4–12% NuPage Bis-Tris gels (Invitrogen) for SDS-PAGE analysis. The gels were transferred using iblot (Invitrogen), and the respective membrane was blocked with 5% Blotto (Bio-Rad Laboratories, Hercules, CA) in TBS-T and incubated with anti-UNC5C antibodies (1:500, MAB1005, R&D systems) and anti-HRP secondaries (mouse-HRP (1:5,000, 31430, Thermo Fisher Scientific), rabbit-HRP (1:10,000, 12-348, EMD Millipore)). Protein was visualized with Supersignal Western Dura extended duration substrate (Thermo Fisher Scientific) and Versa Doc Imaging System (Bio-Rad Laboratories) and quantitated using ImageJ software (NIH).

UNC5C expression on cell surface using flow cytometry. To determine cell surface expression of WT or T835M UNC5C, 293T cells were transiently transfected for 72 h as previously indicated. Live cells were removed from the culture dish with 5 mM EDTA. Subsequently, UNC5C present at the cell surface was labeled with anti-UNC5C antibody, which recognizes the UNC5C extracellular domain (1:500, MAB1005, R&D systems), followed by goat-anti-mouse biotin (1:500, 115-065-166, Jackson ImmunoResearch), and detected with streptavidin-APC (Invitrogen). Samples were analyzed using a FACScan (Becton Dickinson, Franklin Lakes, NJ) and FlowJo software (Tree Star,Inc). Propidium iodide (PI, 1 μg mL^{-1}, Sigma) was used as a viability marker to allow for initial gating on live, single cells.

Aβ ELISA. HEK293 cells stably expressing wild-type human APP695 cells were transfected as previously indicated. At 72 h post-transfection, the conditioned media was collected to assay for APP cleavage products, and cells were lysed using RIPA buffer with Mini-complete Protease Inhibitor Cocktail (Roche) and Phospho-stop (Roche). $Aβ_{x-40}$ and $Aβ_{x-42}$ peptides were measured from cell supernatants by sandwich ELISAs. Briefly, rabbit polyclonal antibody specific for the C terminus of $Aβ_{40}$ (2 μg/ml, AB5737, EMD Millipore) or $Aβ_{42}$ (2 μg/ml, AB5739, EMD Millipore) was coated onto plates, and biotinylated anti-Aβ monoclonal antibody 6E10 (0.05 μg/mL for Aβ 1–40 and at 0.1ug/mL for Aβ 1-42, SIG-39340, Covance, Dedham, MA) was used for detection. The 6E10 epitope lies within amino acids 3–8 of Aβ. Cell lysates were used to confirm equivalent expression levels UNC5C, βgal, and APP (22C11, EMD Millipore), and actin was used as a loading control for each individual experiment.

Extracellular tau assay. HEK293T cells were transiently co-transfected with a human wild-type Tau 441-aa construct and β-gal, WT UNC5C, or UNC5C T835M vector as previously outlined. The conditioned media was collected 72 h post-transfection and assayed for extracellular p-tau or total tau using the MSD 96-Well MULTI-SPOT Alzheimer's disease assay with phospho-tau (Thr231)/total tau with purified neuronal tau calibrators (Mesoscale Discovery). Cell lysates were used to confirm equal expression levels of UNC5C, β-gal and tau, and actin was used as a loading control for each individual experiment.

Time-lapse live-cell imaging. HEK293T cells were transfected as described above. Transfections were incubated for 18 h at 37 °C followed by trypsinization and re-plating into a 96-well plate at 1 $×10^4$ cells $well^{-1}$. Each sample consisted of six replicates, and the experiment was conducted on four separate occasions. Starting at 22 h post-transfection, cells were imaged for GFP or DsRed fluorescence and bright-field at 2–4 h intervals over a 44–64 h period using the IncuCyte^{FLR} or Incucyte^{ZOOM} live cell imaging system (Essen Bioscience). At 66 h post-transfection, total well confluency and GFP confluency were calculated over time using IncuCyte 2011A software (Essen Bioscience). The confluency for each sample was calculated by averaging 3–6 replicates containing at least twelve fields of view. To analyze specific growth of the GFP^+ cells, GFP confluency was divided by total confluency for all time points and best fit lines were created. The slopes of these lines represent specific GFP or DsRed growth. The slope of each sample was then normalized to the respective control within a given experiment.

Cell cycle profile analysis using flow cytometry. HEK293T cells were transfected as previously indicated. The next day, cells were serum starved in media containing 1% serum for 24 h to synchronize. Following this, fresh medium containing full serum (10%) was added to the cells for 24 h. Subsequently, cells were harvested by TrypLE (Gibco) and then washed with PBS containing 5 mM EDTA. Next, cells were fixed with ice-cold 70% ethanol with vortexing and allowed to incubate on ice for 20 min. Cells were then pelleted and washed with PBS with 5 mM EDTA and 1% BSA. Next, cells were treated with PBS containing 5 mM EDTA, 0.5% Tween, 5% goat serum, and 2 μg mL^{-1} RNase (Sigma) for 15min. Following block and permeabilization, cells were incubated for 30 min with anti-UNC5C primary antibody (1:500, sc-135077, Santa Cruz Biotechnology) in staining buffer (PBS with 5 mM EDTA, 0.5% Tween, and 1% BSA) and then washed once with staining buffer. Cells were then resuspended in staining buffer plus goat anti-rabbit biotin (1:500, 111-065-144, Jackson ImmunoResearch Laboratories) and incubated for 30 min on ice. After a single wash with staining buffer, cells were then treated with streptavidin-conjugated APC (1:200, Invitrogen) and 50 μg mL^{-1} PI (Sigma) in staining buffer for 15 min on ice. Subsequently, cells were washed a final time and resuspended in PBS with 5 mM EDTA, 1% BSA, and PI. Samples were analyzed on a BD LSR-II (BD Biosciences) for DNA content of the UNC5C APC^+ population using FlowJo software (Tree Star, Inc.).

Annexin V apoptosis assay using flow cytometry. HEK293T cells were transiently transfected as previously described. At 24 h post-transfection, cells were harvested by TrypLE (Gibco) and washed in FACS buffer (PBS containing 1% BSA and 5 mM EDTA). Following this, cells were resuspended in FACS buffer containing 10 μM Calcein Blue-AM (Invitrogen) and incubated for 15 min. Cells were then pelleted by spinning at 1,400 r.p.m. for 5 min at 4 °C and incubated in annexin V binding buffer (10 mM HEPES, 140 mM NaCl, 2.5 mM $CaCl_2$ pH 7.4) containing PI 1 μg mL^{-1} (Sigma) and annexin V-APC (Invitrogen) for 15 min at room temperature. Subsequently, cells were spun down and resuspended in Annexin V binding buffer with 1 μg mL^{-1} PI. Samples were run on a BD LSR Fortessa cell analyzer (BD biosciences) for the percentage of live, single, GFP^+ cells that showed annexin V staining and analyzed using FlowJo software (Tree Star, Inc.).

Live-cell imaging. HEK293T cells were transiently transfected with β-gal, WT or T835M UNC5C IRES-DsRed constructs as previously described for 24 h, the cells were split into 6 wells of a 96-well precoated poly-D-lysine plate. Caspase activity was monitored by the addition of Cellplayer caspase-3 or caspase-7

activity reagent (1:2,000, Essen Bioscience) to the culture medium. Time-lapse images of HEK293T cells were collected on a Nikon Ti-E inverted microscope with a 20× 0.45-NA objective and Nikon Qi1 camera Nikon Elements software (Nikon Instruments). 293T cells were imaged at 1-h intervals for a minimum of 44 h. Individual cells were identified and tracked over time using the Spots Tracking function in Imaris (Bitplane, Inc). Fluorescence intensities for both the red and green channel for each cell were exported to Excel (Microsoft). Red cells were tracked based on red fluorescent intensity and considered dead upon showing either green fluorescent signal or by loss of red signal. Data represent three independent experiments with six replicates and 24 fields of view per genotype for each experiment.

***In situ* hybridization murine and human samples.** Non-isotopic *in situ* hybridization (ISH) was performed on 4-µm formalin-fixed paraffin-embedded sections using QuantiGene ViewRNA ISH Tissue Assay (Affymetrix/Panomics) following the manufacturer's protocol.

Murine. Gene-specific probe sets were used for detection of *Unc5c* mRNA in mouse (VB1-14659) brain samples, with a probe set to *Bacillus subtilis* dihydropicolinate reductase (dapB) (VF1-11712) used as a negative control, and probe sets specific to mouse Ubiquitin C (VB1-10202) used as a positive control for comparing overall mRNA levels. Alkaline phospatase (AP)-conjugated label probe was used for mouse samples, with Fast Red substrate for chromogenic detection, and hematoxylin was used as a nuclear counterstain.

Human. A gene-specific probe set for detection of human *UNC5C* mRNA (VA1-14551) target region 503–3132 & 7910–8980, GenBank accession NM_003728, was used on tissue samples. A probe set to *Bacillus subtilis* dihydropicolinate reductase (dapB) (VF1-11712)—target region 1363–2044, GenBank accession L38424.1, was used as a negative control. A probe set to human *UBC* (VA1-10203) target region 342–1275, GenBank accession NM_021009, was used as a positive control to preselect tissues with good RNA quality. Deparaffinization was carried out on a Leica stainer XL, and after the boiling step in a Thermo Scientific PT module, the slides were briefly dipped in ethanol and dried before assembling the ISH chamber for the Tecan platform. Warp Fast Red substrate (Biocare) was used for chromogenic detection, and hematoxylin was used as a nuclear counter stain. Hybridized target mRNAs were visualized using bright-field microscopy.

Murine and human mRNA expression. The Animal Care and Use Committee at Genentech approved this study, and use was in accordance with their guidelines. Three 10-month-old male adult age-matched *Unc5c*$^{+/+}$ and three *Unc5c*$^{-/-}$ mice[18] were euthanized by CO_2 followed by cervical dislocation. Hippocampi, cerebellum and cerebral cortices were dissected. Peripheral blood mononuclear cells (PBMCs) were isolated from adult murine spleens and digested with ACK lysis buffer (Invitrogen) to remove red blood cells. Tissue was processed to generate single-cell suspensions and labeled with antibodies to cell surface markers: PE-Cy7-anti-CD3 (1:100, MHCD0312 , Invitrogen), APC-anti-CD11b (1:100, RM2805, Invitrogen), APC-Cy7-anti-CD11c (1:200, A18639, Invitrogen), FITC-anti-CD19 (1:200, RM7701, Invitrogen). SYTOX blue (Invitrogen) was used as a viability indicator, and samples with single-channel fluorescence markers were used to properly set the gates for fluorescent-activated cell sorting (FACSAria, Beckton Dickson) and collecting live, fluorescent positive cells within each indicated PBMC population. Adult human whole blood was acquired from the Genentech Employee Donation Program (informed consent was obtained, and the protocol was reviewed and approved by Western Institutional Review Board. PBMCs were isolated using Lymphoprep and SepMate-50 tube (STEMCELL Technologies, Vancouver, BC, Canada), processed to a single-cell suspension and labeled with the following antibodies to cell surface markers: PECY5- anti-CD3 (1:100, MHCD0318, Invitrogen), FITC-anti-CD14 (1:200, MHCD1401, Invitrogen), AlexaFluor 700-anti-CD11c (1:200, MHCD11C20, Invitrogen), PE-anti-CD19 (1:100, MHCD1912, Invitrogen). They were then sorted in a similar manner to the murine PBMCs samples. RNA was extracted from subdissected regions of murine adult brain or sorted populations of murine or human PBMCs using the RNeasy mini plus kit (Qiagen, Valencia CA). cDNA was synthesized using the cDNA high-capacity reverse transcription kit (Applied Biosystems, Life Technologies, Grand Island, NY), and semiquantitative PCR was performed using TaqMan Gene Expression Master Mix (Applied Biosystems) on a 7500 Real-Time PCR System (Applied Biosystems). PCR primers were murine *Unc5c (*Mm00494093_m1, Invitrogen), murine *Trem2* (Mm04209424_g1, Invitrogen) murine *β-actin* (4352341E, Applied Biosystems); human *Unc5c* (Hs00186620_m1, Invitrogen), human *Trem2* (Hs00219132_m1, Invitrogen), human *β-actin* (4310881E, Applied Biosystems).

Flow cytometry sorting of adult mouse hippocampi and cortex. Both hippocampi or one cortical hemisphere per animal (n = 3 matched pairs of *Unc5c*$^{+/+}$ and *Unc5c*$^{-/-}$) was minced and dissociated with accutase for 20 min at 4 °C. The cells were triturated to single suspension in Hibernate (BrainBits, LLC), passed through a Percoll gradient and then fixed on ice. Cells were blocked in Hibernate and labeled with the following primary antibodies: NueN-488 (1:1,000, MAB377X, Chemicon), GFAP-PE (1:50, 561483, BD Biosciences) and CD11b-APC (1:250, 551282, BD Biosciences) for 30 min at 4 °C. DAPI was added to gate on single cells. The cell-specific subtypes were isolated by FACS and collected for qPCR analysis as described above.

Primary embryonic hippocampal neuron cultures. The Animal Care and Use Committee at Genentech approved this study, and use was in accordance with their guidelines. Timed-pregnant Sprague Dawley rats ere euthanized by CO_2 followed by cervical dislocation. Hippocampi were dissected from embryonic day 18 (E18) rats and enzymatically dissociated using the papain dissociation system following the manufacturer's instructions (Worthington Biochemical Corp, Lakewood, NJ). Dissociated hippocampal cells were placed in nucleofector solution with β-gal, WT or T835M UNC5C IRES-GFP constructs and transduced using the nucleofection method with Amaxa electroporation (Lonza). Following nucleofection, the cells were plated onto precoated poly-D-lysine/laminin plates in NB4Activ medium (BrainBits) supplemented with 1% penicillin/streptomycin (Gibco). The neuronal cultures were challenged with no treatment vehicle (DMSO) control, $A\beta_{1-42}$ (rPeptide), scrambled $A\beta_{1-42}$ peptide (rPeptide), glutamate (Tocris) or staurosporine (Sigma). For $A\beta_{1-42}$, immediately before addition to the culture medium, lyophilized Aβ was resuspended in DMSO then diluted further in neuronal growth media. The neuronal cultures were incubated with Aβ for 48 h and processed for ICC to visualize the GFP-positive transduced neurons. With the experimenter blinded to condition, within three randomly plated wells, ten fields-of-view were captured per well and the number of GFP$^+$ cells was determined by ImageJ automated analysis. In order to compare across conditions and between experiments in which the number of GFP$^+$ transduced cells varied between individual nucleofected vectors, the number of surviving neurotoxin-treated cells was normalized to their respective untreated vector controls.

Time-lapse live-cell imaging. Hippocampal neurons were dissociated and nucleofected as described above. Cells were allowed to attach to poly-D-lysine–coated 96-well plates at 37 °C for 3 h before initiating imaging. Each vector condition consisted of three technical replicates with four-fields-of-view acquired per replicate, and the experiment was conducted on six separate occasions. Five of the independent experiments displayed similar variation. One experiment experienced a technical error of remaining in nucleofector solution too long, and this experiment was discarded due to increased variation within the experiment. Data shown was combined from five experiments that displayed consistent variation across experiments. Starting at 3 h post-nucleofection, cells were imaged for GFP fluorescence and bright field at 4-h intervals for a 116-h period using the IncuCyteZoom live cell imaging system (Essen Bioscience). After 116 h of imaging, number of GFP$^+$ cells per well over time was obtained using IncuCyteZoom 2013A software (Essen Bioscience). The number of cells per well for each sample was calculated by averaging three replicates containing at least 12 fields of view per sample. To determine nucleofection efficiency, the slopes of the best-fit lines for each condition from 0 h to plateau were created. The slopes of these lines represent the rate of vector expression, or nucleofection efficiency. To calculate ongoing basal cell death for each vector, the number of cells remaining at 116 h was divided by the number of cells present at 48 h. Survival of each vector was then normalized to β-gal to capture vector-specific cell death.

doi:10.1038/nm.3736

Statistical analyses. All results are shown as mean ± s.e.m. For every *in vitro* experiment, all samples collected were included in the final analyses. Statistical analysis was performed using either a one-way analysis of variance (ANOVA) or two-tailed *t*-test as indicated using Prism6 software (Graphpad). Data sets were tested for normality using D'Agostino and Pearson omnibus normality test. If data sets did not meet normality, then a nonparametric test was chosen to determine statistical significance. Differences determined to be $P < 0.05$ were considered statistically significant.

30. Purcell, S. *et al.* PLINK: a tool set for whole-genome association and population-based linkage analyses. *Am. J. Hum. Genet.* **81**, 559–575 (2007).
31. Liu, F., Kirichenko, A., Axenovich, T.I., van Duijn, C.M. & Aulchenko, Y.S. An approach for cutting large and complex pedigrees for linkage analysis. *Eur. J. Hum. Genet.* **16**, 854–860 (2008).
32. Abecasis, G.R., Cherny, S.S., Cookson, W.O. & Cardon, L.R. Merlin–rapid analysis of dense genetic maps using sparse gene flow trees. *Nat. Genet.* **30**, 97–101 (2002).
33. Drmanac, R. *et al.* Human genome sequencing using unchained base reads on self-assembling DNA nanoarrays. *Science* **327**, 78–81 (2010).
34. Li, H. & Durbin, R. Fast and accurate short read alignment with Burrows-Wheeler transform. *Bioinformatics* **25**, 1754–1760 (2009).
35. DePristo, M.A. *et al.* A framework for variation discovery and genotyping using next-generation DNA sequencing data. *Nat. Genet.* **43**, 491–498 (2011).
36. Wang, K., Li, M. & Hakonarson, H. ANNOVAR: functional annotation of genetic variants from high-throughput sequencing data. *Nucleic Acids Res.* **38**, e164 (2010).
37. Benitez, B.A. *et al.* TREM2 is associated with the risk of Alzheimer's disease in Spanish population. *Neurobiol. Aging* **34**, 1711 e15–e17 (2013).
38. Cruchaga, C. *et al.* GWAS of cerebrospinal fluid tau levels identifies risk variants for Alzheimer's disease. *Neuron* **78**, 256–268 (2013).
39. Jin, S.C. *et al.* Pooled-DNA sequencing identifies novel causative variants in PSEN1, GRN and MAPT in a clinical early-onset and familial Alzheimer's disease Ibero-American cohort. *Alzheimers Res. Ther.* **4**, 34 (2012).
40. Braak, H. & Braak, E. Neuropathological stageing of Alzheimer-related changes. *Acta Neuropathol.* **82**, 239–259 (1991).
41. Nagy, Z. *et al.* Assessment of the pathological stages of Alzheimer's disease in thin paraffin sections: a comparative study. *Dement. Geriatr. Cogn. Disord.* **9**, 140–144 (1998).
42. Hyman, B.T. & Trojanowski, J.Q. Consensus recommendations for the postmortem diagnosis of Alzheimer disease from the National Institute on Aging and the Reagan Institute Working Group on diagnostic criteria for the neuropathological assessment of Alzheimer disease. *J. Neuropathol. Exp. Neurol.* **56**, 1095–1097 (1997).
43. Price, A.L. *et al.* Principal components analysis corrects for stratification in genome-wide association studies. *Nat. Genet.* **38**, 904–909 (2006).
44. Nelson, C.D. & Sheng, M. Gpr3 stimulates Aβ production via interactions with APP and β-arrestin2. *PLoS ONE* **8**, e74680 (2013).